Relativistic Magnetic Self-Channeling of Light in Near-Critical Plasma: Three-Dimensional Particle-in-Cell Simulation

A. Pukhov* and J. Meyer-ter-Vehn

Max-Planck-Institut für Quantenoptik, Hans-Kopfermann-Strasse 1, 85748 Garching, Germany

(Received 23 October 1995)

We present 3D particle-in-cell simulations for laser pulses with relativistic intensity propagating in slightly underdense plasma. We observe strong flows of relativistic electrons, axially comoving with the pulse. They generate magnetic fields up to 100 MG and strongly influence light propagation. After a phase of filamentation, a single light channel with a width of 1–2 wavelengths is formed by magnetic interaction. A representative case is discussed in which the intensity on axis increases from initially 1.2×10^{19} to 2.0×10^{20} W/cm^2. Ion acceleration and plasma cavitation are also discussed. [S0031-9007(96)00219-0]

PACS numbers: 52.40.Nk, 52.35.Nx, 52.60.+h, 52.65.Rr

A laser beam propagating in underdense plasma with a frequency ω_p smaller than the laser frequency ω undergoes relativistic self-focusing as soon as its total power P exceeds the critical value

$$P_{\mathrm{cr}} \approx 17(\omega/\omega_p)^2 \ \mathrm{GW}; \tag{1}$$

this has been established both theoretically [1] and experimentally [2]. The self-focusing is due to the relativistic mass increase of plasma electrons and the ponderomotive expulsion of electrons from the pulse region. Both effects lead to a local decrease of plasma frequency and an increase in refractive index. The medium then acts as a positive lens. An analysis in terms of the envelope and paraxial approximations [3] shows that, depending on laser pulse and plasma parameters, either self-focusing of the whole pulse or pulse filamentation occurs.

The present paper describes laser light propagation far above threshold (1) and deals with additional effects that become dominant when the dimensionless amplitude $a = eA/mc^2$ of the vector potential A enters the relativistic regime $a > 1$; here, e and m are charge and rest mass of the electron, and c is the velocity of light. The key feature is that the radiation then drives strong currents of relativistic electrons in the direction of light propagation. For single electrons in a plane light wave, the point is well presented in the literature; see, e.g., [4]: As soon as $a > 1$, they are accelerated in forward rather than transverse direction. In plasma below quarter-critical density, plasma waves are exited by stimulated Raman scattering (SRS). It was studied by means of 2D particle-in-cell (PIC) simulations in [5,6] and, in particular, waves resulting from Raman forward scattering were found to produce energetic electrons in the process of wave breaking [7]. The Weibel instability tends to break up these electron flows, forming filaments of fast forward electrons and spatially separated return currents [5]. This current filamentation also leads to light filamentation in addition to the mechanisms discussed above. For driving pulses with $a > 1$, wave breaking and fast electron generation were studied in [8]; in the relativistic regime, the effective plasma frequency decreases, and SRS may set in locally at densities higher than quarter critical. Also, similar electron flows were observed at overdense plasma boundaries [9].

These currents magnetize the plasma. The current densities amount to a sizable fraction f of en_ec and generate quasistatic magnetic fields $B^s_\perp = (fen_e)2\pi r$ at distance r from the axis of a current filament. The field $B^s_\perp$ may become as strong as the magnetic field of the light wave itself, which is $B = aB_0$ in units of $B_0 = mc\omega/e$. For light of wavelength $\lambda = 2\pi c/\omega = 1$ μm, one obtains $B_0 = 107.1$ MG. In units of B_0, the quasistatic magnetic field has the form

$$B^s_\perp/B_0 = (fn_e/n_c)\pi r/\lambda \tag{2}$$

and is of the order B_0 when n_e approaches the critical density $n_c = \pi mc^2/(e\lambda)^2$. We notice that the cyclotron frequency ω_c corresponding to $B^s_\perp$ satisfies $\omega_c/\omega = B^s_\perp/B_0$ and may become resonant with the light frequency, affecting the index of refraction.

In this complex situation, a qualitatively new behavior was observed recently [10]. Based on 2D3V PIC simulations tracing plasma kinetics in two spatial and three velocity dimensions, it was found that the quasistatic magnetic field may become strong enough to pinch the relativistic electrons and that the path of light follows the electron deflection. As a result, the pattern of current and light filaments coalesces into a narrow single channel containing a significant part of the incident laser power. The mechanism of deflecting light by a magnetic field through bending concomitant relativistic electrons was confirmed by applying an external B field [10].

The present work treats this striking phenomenon by PIC simulations in three-dimensional geometry. A representative case with an incident intensity of 1.24×10^{19} W/cm^2 ($a = 3$, $\lambda = 1$ μm) is shown in Fig. 1. It confirms the formation of a single propagation channel with considerably enhanced concentration of light on the axis. The incident beam first propagates through an unstable filamentory stage (blue section in Fig. 1) and then collapses into a single channel with a width

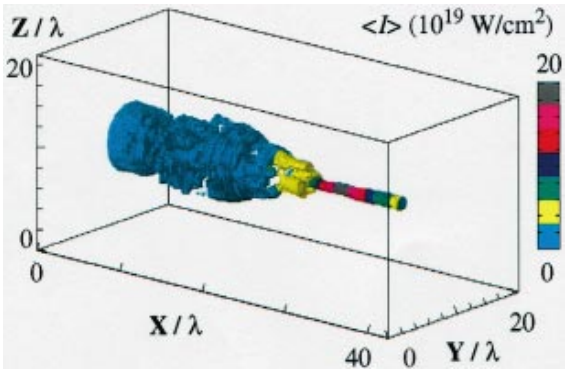

FIG. 1 (color). Perspective view of the self-focusing pulse at time 180 fs. The colors refer to the maximum cycle-averaged light intensity $\langle I_{\max}\rangle$ in each (Y,Z) plane; the plotted surface corresponds to $0.67\langle I_{\max}\rangle$.

of $(1-2)\lambda$. We present details of this simulation and similar ones with different parameters. To the best of our knowledge, no *three-dimensional* PIC simulations of relativistic self-focusing have been published so far.

For the numerical simulation of laser plasma interaction in this regime, the fully relativistic electromagnetic 3D3V PIC code LPLAS3D has been developed at the Max-Planck-Institute for Quantum Optics. It is a 3D generalization of the 2D3V code LPLAS2D [8,10,11]. It uses a spectral representation of fields [12,13], thereby insuring correct dispersion of electromagnetic waves with phase velocity $V_{\rm ph} \equiv c$ in vacuum and $V_{\rm ph} > c$ in plasma regions. It describes arbitrarily relativistic particles without any numerical Cherenkov radiation [12,13]. We mention that the paraxial and envelope approximations as well as hydrodynamic modeling are insufficient to treat the effects discussed in the present paper; structures on the scale of a wavelength are involved and non-Maxwellian velocity distributions demanding a kinetic treatment.

The simulation box is indicated in Fig. 1. The laser beam with a diameter of 12λ and a Gaussian intensity profile is incident from the left. The corresponding Rayleigh length is $R \approx 110\lambda$. The pulse amplitude rises according to $a = 0.5[1 + \tanh(\omega t/40)]a_0$ with $a_0 = 3$. We choose a relatively sharp leading front of 6λ from the very beginning to save simulation time, as simulations with smoother pulses and present parameters show formation of sharp fronts anyhow later during the interaction. The incident pulse is linearly polarized along the Z axis. Initially, the volume between $0 \le X/\lambda \le 5$ is vacuum; between $5 \le X/\lambda \le 41$, it is filled with uniform hydrogen plasma of density n_0. High densities are of particular interest here [see Eq. (2)], and we choose $n_0/n_c = 0.36$, still undercritical to insure propagation. As to the fields, boundary conditions in the X direction correspond to beam incidence at $X = 0$ and beam absorption behind the plasma, while escaping particles are stopped at the boundaries and returned with the background temperature. In the Y and Z directions, periodic boundary conditions are chosen. We used a spatial mesh of $256 \times 128 \times 128$ cells and up to 10^7 electrons and ions (ion mass is $1836m$). This amounts to 2 electrons and 2 ions per cell initially and 6 grid points per λ. Being fairly rough, this is found to be the lower limit consistent with an acceptable noise level for the physics studied here. We use the small time step $\tau = 0.3/\omega$. This resolves the important figure-8 motion of electrons in vacuum. An initial electron temperature of 20 keV was chosen for numerical reasons. For the physical cases considered here, such a temperature is still far below the quiver energy and therefore acceptable. The code was run on a high-performance RISC workstation IBM RS/6000 7015/R24 with 1 GB main memory. A typical run needs 50 h CPU time. Plasma volume and time interval are limited by memory and CPU. Use of a massively parallel computer is planned [14].

Results of the simulation are presented in longitudinal (Fig. 2) and transverse (Fig. 3) cuts through the plasma volume. Figures 2(a) and 2(b) illustrate the initial stage of laser pulse filamentation and magnetic field generation at 80 fs; the quantities plotted in colors are (a) the instantaneous intensity $I = c(E^2 + B^2)/8\pi$ and (b) the low-frequency (quasistatic) part of the magnetic field component B_z^s, average over 1.5 laser periods. Notice the sharp pulse front with thickness $\approx 1\lambda$ in Fig. 2(a), much less than the initial 6λ. The onset of filamentation is most clearly seen in vertical cut I (first row in Fig. 3): The intensity I (first column) reveals strong fluctuations, the averaged transverse magnetic field $B_\perp^s$ (second column) has a ringlike form and corresponds to a longitudinal current J_x (third column) which has been plotted in normalization form $J_x = e(n_i v_{x_i} - n_e v_{x_e})/en_0c$. The J_x plot shows bluish current filaments of fast electrons streaming with the light (negative J_x due to negative electron charge) and in between brownish regions filled by return currents of cold background electrons. The currents amount to $\approx 0.5en_0c$ and generate peak magnetic fields between 50 and 100 MG in agreement with Eq. (2).

Filamentation is more clearly seen at the beam front in Fig. 2(a). The three beam filaments actually correspond to a ring and a central filament, as one learns from the transverse plots in the second row of Fig. 3 (cut II). Also quite regular ringlike structure are seen in $B_\perp^s$ and J_x with alternating forward and return current sheets. One should notice that the radial extent of these distributions shrinks toward the beam front. Following [10], we attribute this contraction to the magnetic field that pinches the electron current; the light channels follow the currents, guided by the refractive index modified by the fast electrons.

Figures 2(c) and 2(d) display beam evolution at a later stage at 320 fs. In the longitudinal intensity cut, one observes how the beam contracts through different phases of radial filamentation and finally merges into one central filament. In the transverse cuts, this corresponds to a ring at cut III and eventually to a single channel at cut IV. This is the central result of this paper. Varying beam intensity, we find that this kind of single channel formation occurs for incident amplitudes $a \ge 1$. The threshold behavior

has still to be studied in more detail. Certainly, also high plasma density is required to generate high enough magnetic fields sufficient for pinching the beam.

An important feature is plasma cavitation. It is seen in the ion density plotted in Fig. 2(d). The expulsion of electrons from the region of high beam intensity generates an electrostatic field which accelerates the ions in radial direction. We find ion energies up to 3 MeV in the simulation. An outgoing collisionless shock is observed. In the region of tightest focusing, the ion density on axis is almost zero. The cross section of the ion channel is almost circular. Such channel formation in plasma has been seen in 2D PIC simulations; see, e.g., [9,15]. In 3D geometry, the effect becomes more prominent.

Both linear and circular polarization lead to single channel formation. Linear polarization has the effect that the distributions of J_x and $B_\perp^s$ at the positions of tight focusing (cuts III, IV in Fig. 3) are elongated in the direction of polarization. We find that the electrons are accelerated mainly in the plane of polarization in the forward direction, but with a certain angular spread relative to the beam axis. Their distribution in energy resembles a thermal spectrum with a temperature between 3 and 5 MeV, similar to 2D results [5]. Surprisingly, the light beam stays tightly focused with a circular cross section. This is interpreted in Fig. 4. We show (a) the electron density in terms of $(\omega_p/\omega)^2$ and (b) the quantity $(\omega_p/\omega)^2\langle\gamma^{-1}\rangle = 1 - n_r^2$, related to the refractive index n_r obtained from linear theory with a local average $\langle\gamma^{-1}\rangle$ of the relativistic γ factor. Comparing the two plots, the effect of heavy relativistic electrons sprayed in the direction of polarization [green area in Fig. 4(b)] is evident; nevertheless, the effect of density cavitation (dark blue area) on n_r dominates and guides the light beam. We also checked the direct effect of the magnetic field on the refractive index. It is expected in regions where the **E** vector of the light is perpendicular to the $\mathbf{B}_\perp^s$ field. We find that it plays a role in the intermediate stages of the filamentation and contributes to the formation of the central channel.

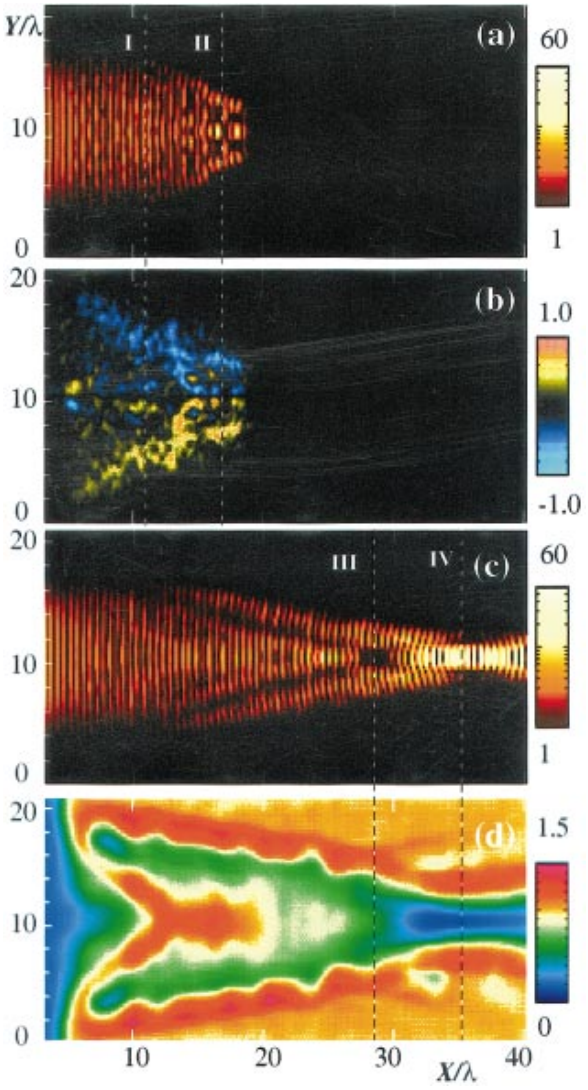

FIG. 2 (color). Longitudinal (X,Y) cuts along the pulse axis: (a),(c) instantaneous light intensity I (10^{19} W/cm^2, logarithmic color scale); (b) quasistatic magnetic field B_z (10^8 G); (d) ion density n_i/n_0. (a),(b) refer to time $t_1 = 80$ fs and (c),(d) to $t_2 = 320$ fs. Dashed lines I–IV mark transverse cuts shown in Fig. 3.

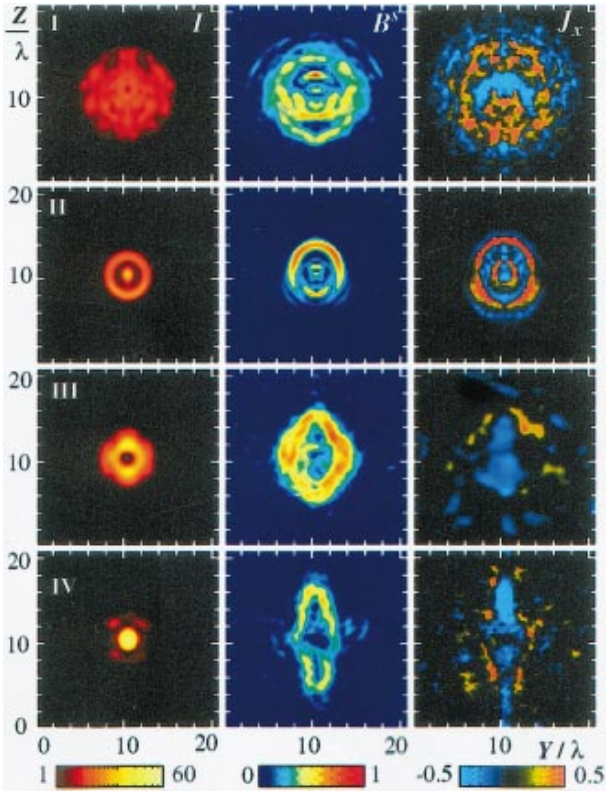

FIG. 3 (color). Transverse (Y,Z) cuts I–IV at X positions and times given in Fig. 2. The columns show I (10^{19} W/cm^2, logarithmic color scale), the transverse magnetic field $B_\perp^s$ (10^8 G), and the longitudinal current J_x in units of en_0c, respectively. Color scales are given below each column. Notice that the E field introduces an up (down) asymmetry in these snapshots; the tiny left (right) asymmetry is due to noise.

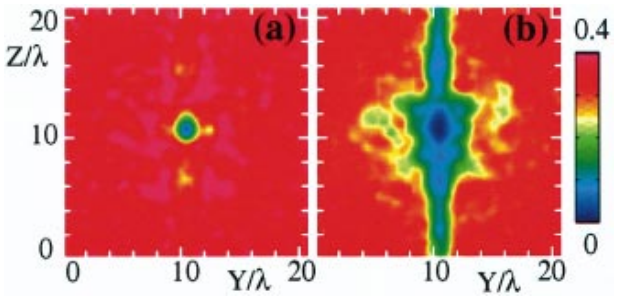

FIG. 4 (color). Transverse (Y,Z) plots at cut IV of (a) $(\omega_p/\omega)^2 = (4\pi e^2/m\omega^2)n_e$ and (b) $(\omega_p/\omega)^2\langle\gamma^{-1}\rangle$.

In Fig. 5, we show (a) the beam intensity on axis and (b) the total beam power P_t vs X. The beam power is obtained by integrating the Poynting vector across the vertical plane. The full 3D result is compared with the case of fixed ions and with 2D simulations, propagating a slab of laser light of the same initial width through an identical plasma and assuming either s or p polarization (parallel or normal to plane of slab). It is seen that the full 3D simulation including ion motion gives by far the highest light intensities on axis. Losses are smallest for propagation through the channel with depleted plasma density. As the ion channel develops, the point of maximum intensity moves forward.

In conclusion, we have presented first 3D PIC simulations of short-pulse laser propagation in near-critical plasma at relativistic intensities. They show the formation of a single magnetized light channel, carrying light as well as strong axial currents and quasistatic magnetic fields. These fields survive after the driving pulse has passed [16] and will decay over some 100 ps due to collisions. Plasma cavitation is found along the channel. Hole boring into overdense plasma is a key feature for fast ignition of fuel targets in the context of inertial confinement fusion [17]. Implications of the present results in this respect have still to be studied.

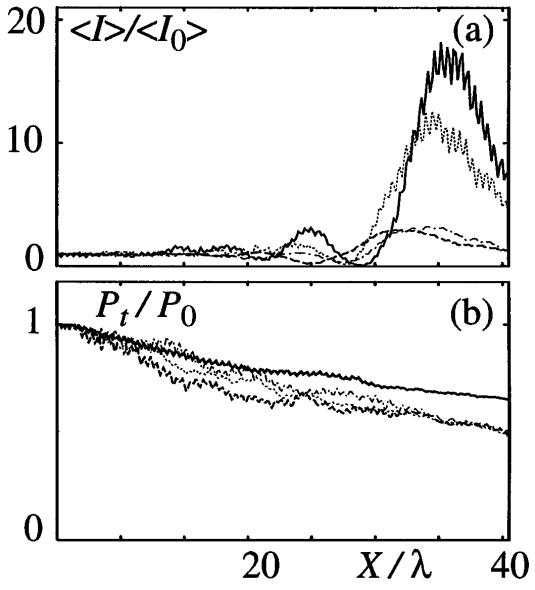

FIG. 5. (a) Cycle-averaged light intensity on axis $\langle I\rangle$ and (b) total beam power P_t, both normalized to incident values $\langle I_0\rangle$ and P_0, at time $t_2 = 320$ fs for different simulated cases: 3D with moving ions (solid line), 3D with fixed ions (points), 2D p polarized (dashes), 2D s polarized (dash-dots).

We would like to thank S. V. Bulanov and F. Pegoraro for stimulating discussions. J. M. t. V. acknowledges a discussion with M. Tabak concerning magnetic focusing. A. P. thanks the Max-Planck-Institut für Quantenoptik for its hospitality. This work was supported in part by the Bundesministerium für Forschung und Technologie, by EURATOM, and by HCM under Contract No. ERB 4050 PL93 0338.

*Permanent address: Moscow Institute for Physics and Technology, Dolgoprudnyi, Moscow Region, Russia.

[1] C. E. Max, J. Arons, and A. B. Langdon, Phys. Rev. Lett. **33**, 209 (1974); H. Hara, J. Opt. Soc. Am. **65**, 882 (1975); G. Sun *et al.*, Phys. Fluids **30**, 526 (1987); P. Sprangle *et al.*, IEEE Trans. Plasma Sci. **PS-15**, 145 (1983); G. Schmidt and W. Horton, Comments Plasma Phys. Controlled Fusion **9**, 85 (1985); A. B. Borisov *et al.*, Phys. Rev. A **45**, 5830 (1992).
[2] A. B. Borisov *et al.*, Phys. Rev. Lett. **68**, 2309 (1992); P. Monot *et al.*, Phys. Rev. Lett. **74**, 2953 (1995).
[3] A. B. Borisov *et al.*, Plasma Phys. Controlled Fusion **37**, 569 (1995).
[4] E. S. Sarachik and G. T. Schappert, Phys. Rev. D **1**, 2738 (1970); P. B. Corkum, N. H. Burnett, and F. Brunel, in *Atoms in Intense Laser Fields*, edited by M. Gavrila (Academic Press, New York, 1992), p. 109.
[5] D. W. Forslund *et al.*, Phys. Rev. Lett. **54**, 558 (1985).
[6] W. B. Mori *et al.*, in *Proceedings of the 7th International Workshop on Laser Interaction and Related Plasma Phenomena, Monterey, CA, 1985*, edited by H. Hora and G. Miley (Plenum Press, New York, 1986), Vol. 7, p. 767.
[7] C. D. Decker *et al.*, Phys. Rev. E **50**, R3338 (1994).
[8] S. V. Bulanov, F. Pegoraro, and A. M. Pukhov, Phys. Rev. Lett. **74**, 710 (1995).
[9] G. A. Askar'yan *et al.*, Phys. Rev. Lett. **69**, 1383 (1992).
[10] G. A. Askar'yan *et al.*, JETP Lett. **60**, 251 (1994).
[11] S. V. Bulanov, F. Pegoraro, and A. M. Pukhov, Phys. Lett. **195A**, 84 (1994).
[12] J. Dawson, Rev. Mod. Phys. **55**, 403 (1983).
[13] C. K. Birdsall and A. B. Langdon, *Plasma Physics via Computer Simulations* (Adam Hilger, New York, 1991).
[14] J. Dawson, Phys. Plasmas **2**, 2189 (1995), and references therein.
[15] W. B. Mori *et al.*, Phys. Rev. Lett. **60**, 1298 (1988).
[16] S. V. Bulanov *et al.*, Phys. Rev. Lett. **76**, 3562 (1996).
[17] M. Tabak *et al.*, Phys. Plasmas **1**, 1626 (1994).